Subsea jumper damage detection based on fractal analysis and modal characteristics

Yan Li[1], XingKun Zhou[1,2]*, WenHua Li[1,2]

[1] Department of Marine Engineering, Dalian Maritime University, 116026 Dalian, P.R China

[2] National Center for International Research of Subsea Engineering Technology and Equipment, Dalian Maritime University, Dalian, P.R China

ARTICLE INFO

ABSTRACT

Subsea jumpers play a critical role in subsea oil and gas production. Structural damage such as cracks is inevitable in subsea jumpers due to the harsh marine environment (internal fluid flow corrosion, high temperature and pressure, etc.). However, the current research on damage detection and evaluation of subsea jumpers is limited, particularly in cases of slight damage. This study thus proposes a method to identify cracks in subsea jumpers based on the modal characteristics and fractal theory. The accuracy of the method is verified by comparing the finite element simulation method via APDL and the analytical method via MATLAB. In addition, the sensitivity of the method to noise is investigated. The results indicate that the method accurately identifies cracks (single and multiple) with a minimum depth of 0.2 mm in various locations on subsea jumpers. This study may hold significant reference value for improving the safety and reliability of subsea jumpers.

1. Introduction

Subsea jumpers are critical for connecting components within subsea oil and gas production systems, such as Christmas trees, manifolds, pipeline terminals, and risers. However, extended exposure to ocean currents inevitably induces vortex-induced vibrations, resulting in stress concentration and fatigue damage, leading to crack formation [1]. In addition, the transportation of multiphase mixtures can subject subsea jumpers to cyclic stress due to the oscillations of gas and liquid plugs, potentially causing pipeline instability, decreased strength, and fatigue damage [2-6]. Therefore, monitoring and maintaining jumpers is crucial for the long-term safety and reliability of subsea oil and gas production systems.

Traditional damage detection of subsea jumpers relies primarily on conventional visual, ultrasonic, and magnetic leakage methods, etc. However, these traditional methods have some limitations in application, such

---

as high operating costs and the lack of global monitoring capability. Therefore, a need exists to develop a reliable and cost-effective method for global damage detection of subsea jumpers.

Vibration-based structural health monitoring is a widely used technology for structural damage detection. Initially, modal parameters such as natural frequency and modal curvature were often used to detect structural damage [7, 8]. Subsequently, modal strain energy became widely used to detect damage in various structures, such as steel frames [9], bridges [10, 11], offshore platforms [12], and wharves [13]. Numerous studies now combine modal parameters with artificial intelligence or other algorithms to detect structural damage [14-16].

Due to the low cost of numerical simulation and easy extraction and analysis of large quantities of data, the vibration-based damage detection method is increasingly applied to marine risers [17-19]. For instance, Zhou et al. [20] used transfer matrix techniques to extract patterns and detect damage in marine risers, then identified cracks incurred during riser deployment and retrieval [21]. In other work, Bayik et al. [22] introduced a laboratory-scale model for studying vibration-based damage detection in a top-tensioned riser.

It was not until the 20th century that fractal theory was extended to damage detection. Hadjileoniadis et al. [23] used fractal dimensions to process first-order modal parameters and detect damage in cantilever beams and supported rectangular plates. Qiao and Cao [24] then proposed the modal anomaly algorithm, which addresses the limitations of fractal dimension in high-order damage detection. Bai et al. [25] proposed a two-dimensional fractal-dimension operator method that uses the same approach to identify cracks in plates. Huang et al. [26] used a multitask sparse Bayesian learning approach and the Katz dimension to predict damage location.

In contrast with current studies on damage detection of marine structures, which primarily concentrate on risers, the present study proposes a damage detection approach based on vibration theory to detect damage in subsea jumpers. This study uses modal analysis to extract the modal parameters and then applies fractal theory for damage detection. The proposed method verifies the effectiveness by identifying single and multiple cracks of varying depths and at different positions on subsea jumpers. In addition, the robustness of the method to withstand noise is analyzed.

This paper is structured as follows: Section 2 introduces the numerical model of the jumper and the crack identification theory. Section 3 presents the model calculation and verification through comparative analysis. Section 4 analyzes and discusses the results, including the presence of noise. Finally, Section 5 presents the conclusions.

2. Free vibration theory of subsea jumpers and crack identification technique

Fig. 1 Typical M-type subsea jumper

This study investigates M-type subsea jumpers (see Fig. 1), which are widely used due to their facile manufacture and installation, low cost, and broad applicability at different depths. The susceptibility to bending stress of bent pipes during operation means that plastic deformation, cracking, and even fracture may occur when the bending stress exceeds the material's strength [27]. Therefore, the damage location of the subsea jumper assumed in this study is concentrated on the bent pipes (see red region in Fig. 2).

2.1 Numerical model of subsea jumper

Fig. 2 shows the model of the subsea jumper studied in this paper taken from Li et al. [28]. The jumper is made of X65 steel, as per API Spec 5L [29].
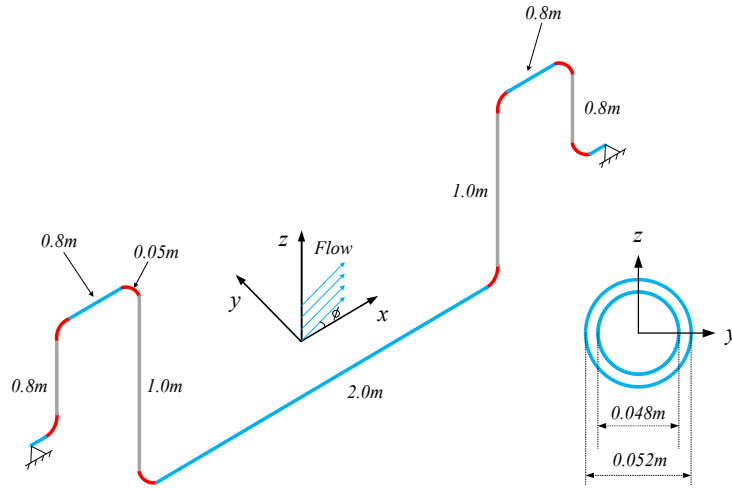
Fig. 2 Subsea jumper model in global coordinate system

(a)	(b)
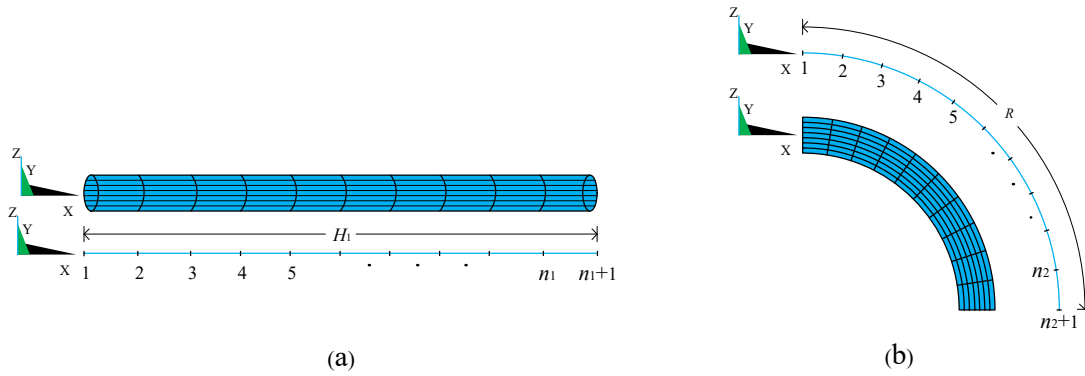
Fig. 3 (a) Elements and nodes of the straight-pipe model, (b) Elements and nodes of the bent-pipe model

Referring to the classical Euler-Bernoulli beam theory, the jumper structure can be equivalent to a series of three-dimensional Euler-Bernoulli beam elements [30]. Fig. 3 shows the discretization elements and nodes for straight and bent pipes in the jumper. The degrees of freedom of each element are shown in Fig. 4. The stiffness and mass matrixes of the jumper are computed, followed by a modal analysis of the system.
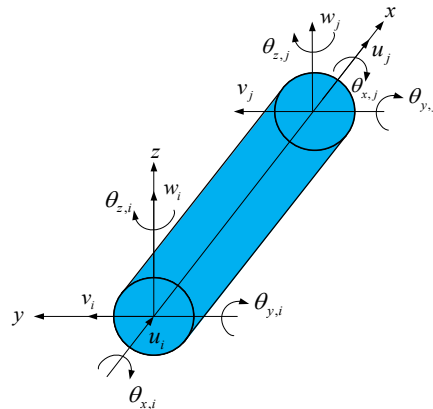
Fig. 4 Degrees of freedom of three-dimensional Euler-Bernoulli beam

The degrees vector of freedom of the beam element e can be expressed as:

$$e = [u_i \ \ v_i \ \ w_i \ \ \theta_{x,i} \ \ \theta_{y,i} \ \ \theta_{z,i} \ \ u_j \ \ v_j \ \ w_j \ \ \theta_{x,j} \ \ \theta_{y,j} \ \ \theta_{z,j}]^T \tag{1}$$

The axial displacement u of the beam element is:

$$u = N_u e \tag{2}$$

where N_u is:

$$N_u = [1 - \frac{x}{l} \ \ 0 \ \ 0 \ \ 0 \ \ 0 \ \ 0 \ \ \frac{x}{l} \ \ 0 \ \ 0 \ \ 0 \ \ 0 \ \ 0] \tag{3}$$

The transverse displacements v and w of the beam element are:

$$\begin{bmatrix} v \\ w \end{bmatrix} = N_l e \tag{4}$$

The shape function matrix N_l is given as:

$$N_l = \begin{bmatrix} 0 & N_1 & 0 & 0 & 0 & N_2 & 0 & N_3 & 0 & 0 & 0 & N_4 \\ 0 & 0 & N_1 & 0 & -N_2 & 0 & 0 & 0 & N_3 & 0 & -N_4 & 0 \end{bmatrix} \tag{5}$$

The expressions of N_1, N_2, N_3, N_4 are:

$$N_1 = 2(\frac{x}{l})^3 - 3(\frac{x}{l})^2 + 1 \tag{6}$$

$$N_2 = l(\frac{x}{l})^3 - 2l(\frac{x}{l})^2 + x \tag{7}$$

$$N_3 = 3(\frac{x}{l})^2 - 2(\frac{x}{l})^3 \tag{8}$$

$$N_4 = l(\frac{x}{l})^3 - l(\frac{x}{l})^2 \tag{9}$$

The torsion angle of the beam element θ_x is:

$$\theta_x = N_\theta e \tag{10}$$

where N_θ is:

$$N_\theta = \begin{bmatrix} 0 & 0 & 0 & 1 - \frac{x}{l} & 0 & 0 & 0 & 0 & 0 & \frac{x}{l} & 0 & 0 \end{bmatrix} \tag{11}$$

Using the shape function matrices (3), (5), (11), the stiffness matrix of the beam element is calculated according to the Euler-Bernoulli beam theory:

$$K_N^e = \int_0^l \begin{bmatrix} N_u' \\ N_l'' \\ N_\theta \end{bmatrix}^T D_K \begin{bmatrix} N_u' \\ N_l'' \\ N_\theta \end{bmatrix} dx \tag{12}$$

where $D_K = \text{diag}(EA, EI, EI, GJ)$. Table 1 lists the values of E, EI, and GJ. The superscript $'$ in Eq. (12) indicate derivation with respect to x.

Table 1 Main physical properties of the subsea jumper.

Parameter	Value	Units
Elastic modulus (E)	200	GPa
Bending stiffness (EI)	1.97×10^4	N·m^2
Shear modulus (G)	76.9	GPa
Torsional stiffness (GJ)	1.51×10^4	N·m/deg

Similarly, the mass matrix of the beam element is:

$$\boldsymbol{M}_N^e = \int_0^l \boldsymbol{N}^T \boldsymbol{D}_M \boldsymbol{N} \mathrm{d}x \tag{13}$$

where $\boldsymbol{D}_M = \mathrm{diag}(m, m+m_a, m+m_a, mJ/A)$, with m being the element mass, while $m_a = C_a \rho \pi D^2 / 4$ is the potential additional mass. Matrix $\boldsymbol{N} = [\boldsymbol{N}_u^T \quad \boldsymbol{N}_l^T \quad \boldsymbol{N}_\theta^T]^T$ represents the complete shape function matrix for the beam element.

Assuming that the jumper is linear and damping is negligible, the free vibration equation of the jumper is:

$$\boldsymbol{M}_N^e \ddot{e}(t) + \boldsymbol{K}_N^e e(t) = 0 \tag{14}$$

The characteristic matrix must be transformed by a coordinate transformation into the overall coordinate system. The free vibration equation of the jumper is:

$$\widetilde{\boldsymbol{M}}_N^e \ddot{\tilde{e}}(t) + \widetilde{\boldsymbol{K}}_N^e \tilde{e}(t) = 0 \tag{15}$$

where $\widetilde{\boldsymbol{M}}_N^e = \boldsymbol{T} \boldsymbol{M}_N^e \boldsymbol{T}^T$ and $\widetilde{\boldsymbol{K}}_N^e = \boldsymbol{T} \boldsymbol{K}_N^e \boldsymbol{T}^T$. The coordinates transformation matrix $\boldsymbol{T} = \mathrm{diag}(\boldsymbol{G}, \boldsymbol{G}, \boldsymbol{G})$, where the transformation matrix $\boldsymbol{G}$ is:

$$\boldsymbol{G} = \begin{bmatrix} \cos(x,X) & \cos(y,X) & \cos(z,X) \\ \cos(x,Y) & \cos(y,Y) & \cos(z,Y) \\ \cos(x,Z) & \cos(y,Z) & \cos(z,Z) \end{bmatrix} \tag{16}$$

Eq. (15) can be expanded as follows:

$$\sum_{j=1}^n m_{ij} \ddot{\tilde{e}}_j(t) + \sum_{j=1}^n k_{ij} \tilde{e}_j(t) = 0 \qquad (i,j=1,2,3,\cdots,n) \tag{17}$$

where n is the number of degrees of freedom of the structure. Let the synchronous solution of the jumper be given as:

$$\tilde{e}_j(t) = h_j f(t) \qquad (j=1,2,3,\cdots,n) \tag{18}$$

where h_j is a set of constants, $f(t)$ is a time-dependent function. Make $\omega_n^2 = \sum_{j=1}^n k_{ij} h_j \bigg/ \sum_{j=1}^n m_{ij} h_j$, substitute and organize to obtain:

$$\ddot{f}(t) + \omega_n^2 f(t) = 0 \tag{19}$$

$$\sum_{j=1}^n (k_{ij} - \omega_n^2 m_{ij}) h_j = 0 \tag{20}$$

Eq. (20) in matrix form is:

$$(\boldsymbol{k} - \omega_n^2 \boldsymbol{m})\boldsymbol{h} = 0 \tag{21}$$

Eq. (21) defines an *n*-dimensional generalized eigenvalue problem and can be rewritten as a standard eigenvalue problem:

$$(\boldsymbol{D} - \lambda \boldsymbol{I})\boldsymbol{h} = 0 \tag{22}$$

where $\boldsymbol{D} = \boldsymbol{k}^{-1}\boldsymbol{m}$. The characteristic values of Eq. (22) are:

$$\lambda = \frac{1}{\omega_n^2} \tag{23}$$

Because h_j has a nonzero solution, the frequency governing equations are:

$$\left| \boldsymbol{k} - \omega_n^2 \boldsymbol{m} \right| = 0 \tag{24}$$

$$\left| \boldsymbol{D} - \lambda \boldsymbol{I} \right| = 0 \tag{25}$$

where $\lambda = 1 / \omega_n^2$ is the characteristic root of the equation, ω_n is the *n*th-order natural frequency, and $\boldsymbol{h}$ is the modal displacement vector. Expanding Eq. (25) to obtain the *n*th-degree algebraic equation about the eigenvalue root λ:

$$a_1 \lambda^n + a_2 \lambda^{n-1} + \cdots + a_{n-1} \lambda + a_n = 0 \tag{26}$$

If no duplicate roots exist, the *n* roots of λ ranked in order of size are $\lambda_1 > \lambda_2 > \cdots > \lambda_{n-1} > \lambda_n$

The corresponding natural frequencies are $\omega_{n1} < \omega_{n2} < \cdots < \omega_{nr} < \omega_n$, where ω_{nr} is the *r*th natural frequency of the structure and can be substituted into Eq. (22) to obtain the corresponding *r*th modal displacement vector $\boldsymbol{h}^{(r)}$. The natural frequency ω_{nr} and modal displacement vector $\boldsymbol{h}^{(r)}$ constitute the *r*th natural mode.

Before detecting damage, it is necessary to normalize the data to ensure rapid and precise damage detection while mitigating the data complexity. The normalized expression for the modal displacement is:

$$\bar{\boldsymbol{h}} = \frac{\boldsymbol{h}}{\max(|\boldsymbol{h}|)} \tag{27}$$

2.2 Crack modeling

When cracks occur on the surface of the subsea jumper, the strain energy concentrates around the cracks and modifies the local flexibility. Although the crack's displacement is continuous at both ends, the rotation angle is not continuous. According to the literature [31-33], a torsional spring is often used to simulate the above behaviors of cracks, where the stiffness of the cracked element is equated with the spring stiffness. Based on previous studies [31-33] and using the parameters in Table 1 and Fig. 2, the equivalent stiffness G_c of the cracked element is:

$$G_c = \frac{1}{C} \tag{28}$$

where *C* is the flexibility coefficient of the cracked section, which is:

$$C = \frac{1024}{\pi E D_o^3 (1 - \gamma^4)^2} \int_0^{a_c/D_o} \{ \int_{-\sqrt{x-x^2}}^{\sqrt{x-x^2}} (1 - 4y^2)(2x + \sqrt{1 - 4y^2} - 1) F'^2 \, dy \} dx \tag{29}$$

where a_c is the crack depth, $\gamma = D_o/D_i$, $x = \xi/D_o$, $y = \eta/D_o$, and F' is a function of the local relative position x'.

$$F' = \frac{\sqrt{2/\pi x' \tan \pi x'/2}[0.923 + 0.199(1 - \sin \pi x'/2)^4]}{\cos \pi x'/2} \tag{30}$$

where $x' = \left(2x + \sqrt{1 - 4y^2} - 1\right)\big/\left(2\sqrt{1 - 4y^2}\right)$. The cracks of different depths can be simulated by changing the stiffness of the torsional spring.

Figs. A.1 and A.2 of Appendix A show the schematic diagram and formula letters of the cracked element of the jumper and the cracked node number diagram, respectively.

2.3 Damage detection technique

Fractal theory is a relatively new realm of nonlinear chaos research that extends Euclidean theory and supplements calculus [34]. The irregularity of the structures can be quantified via their fractal dimension (FD). Since damage often involves local irregularities in the shape of structures, using FD to process data constitutes a practical and effective means to assess the integrity of structures.

This study uses the Katz fractal dimension (KFD). Hadjileontiadis et al. [23] proposed using the FD-based crack-detector (FDCD) method when using KFD for structural damage detection. The typical expression for KFD is:

$$KFD(x) = \frac{\log_{10}(n)}{\log_{10}\left(\dfrac{d(x)}{L(x)}\right) + \log_{10}(n)} \tag{31}$$

where $d(x)$ is the maximum distance between the first sample point and the remaining sample points in the sliding window. $L(x)$ is the sum of the lengths of the lines of adjacent sampling points, and n (usually even) is the number of sample distances in the sliding window.

A sliding window of $n = 4$ serves to explain Eq. (31) (see Fig. 5).
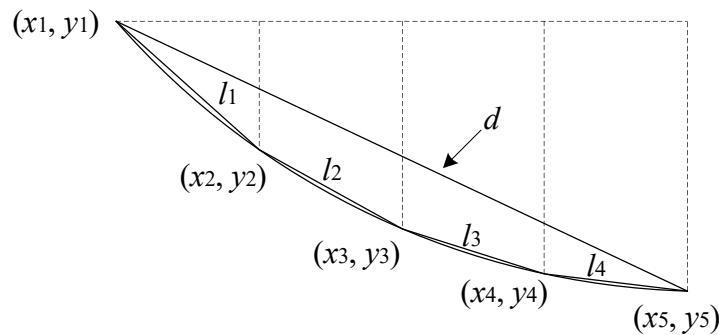
Fig. 5 A sliding window with four sample distances centered on (x_3, y_3)

The effect of damage detection may depend on the sample distance and the number of sample points in a sliding window. The sample distance and the number of sample points should be chosen multiple times and results compared to maximize detection efficacy. Fig. 6 shows a flow chart of the complete damage detection procedure.
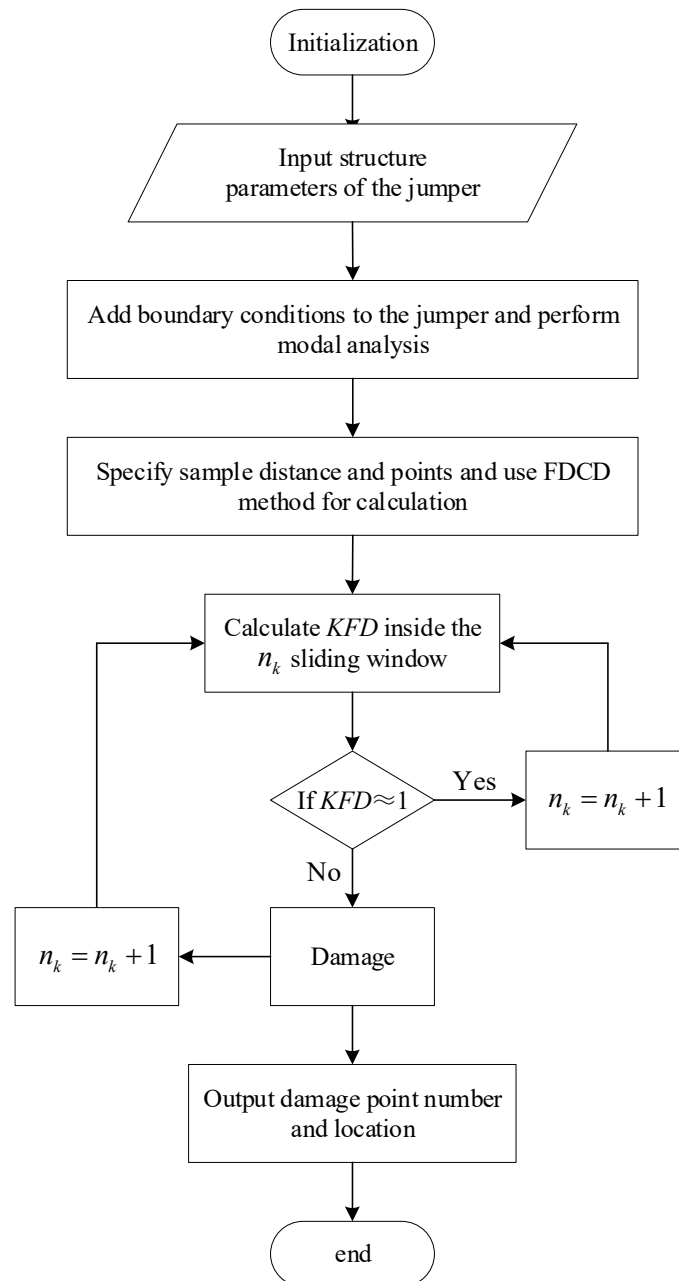
Fig. 6 Flowchart of the FDCD method for damage detection

3. Solution and Verification

This section models and calculates the jumper model presented in Section 2. Fig. 7 shows the discretized model of the jumper in the *x-z* plane. The calculation program was coded and redeveloped using APDL (ANSYS Parametric Design Language) in ANSYS commercial software. We used the PIPE288 element type in the ANSYS software to exploit its advantageous properties, such as additional mass (especially with ocean loads), which enables fluid dynamics calculations involving fluid masses and buoyancy loads. Marine environment loads due to seawater, waves, and currents can be simulated using commands such as OCTYPE, OCDATA, and OCTABLE [35].
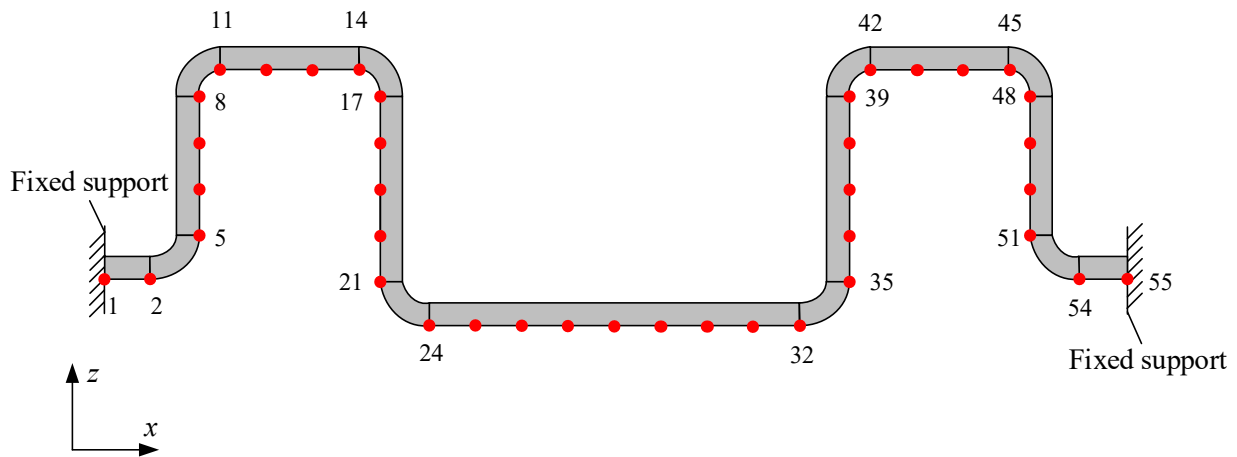
Fig. 7 Discrete element diagram of the overall structure of the jumper

To verify the accuracy of this approach, we applied a modal analysis to the jumper model proposed by Wang et al. [36] and compared the natural frequencies with those obtained in related studies. Given the discretization model in this study, we used the Block Lanczos method for modal calculations in APDL and the Krylov subspace algorithm in MATLAB. Tables 2 and 3 and Figs. 8 and 9 compare the natural frequencies and normalized modal data obtained through each method.

Table 2 Calculation natural frequencies of the jumper model based on Wang et al.

MODE	This study	Qu et al. [30]	Zheng et al. [37]
1	0.845	0.848	0.863
2	2.137	2.141	2.149
3	2.225	2.200	2.194
4	2.588	2.575	2.542
5	3.262	3.285	-
6	3.622	3.606	-
7	3.678	3.644	-
8	6.198	6.195	-

Table 3 Comparison and verification of the two methods used in this study.

MODE	Healthy (via APDL)	Healthy (via MATLAB)	Damaged (via APDL)	Damaged (via MATLAB)
1	4.7038	4.7038	1.0642	1.0642
2	7.8315	7.8315	4.1916	4.1916
3	10.5788	10.5788	4.6266	4.6266
4	10.6477	10.6477	8.6574	8.6574
5	10.8115	10.8115	9.7714	9.7714
6	17.1235	17.1235	10.6153	10.6153
7	17.5105	17.5105	15.9225	15.9225
8	37.0754	37.0754	17.1229	17.1229
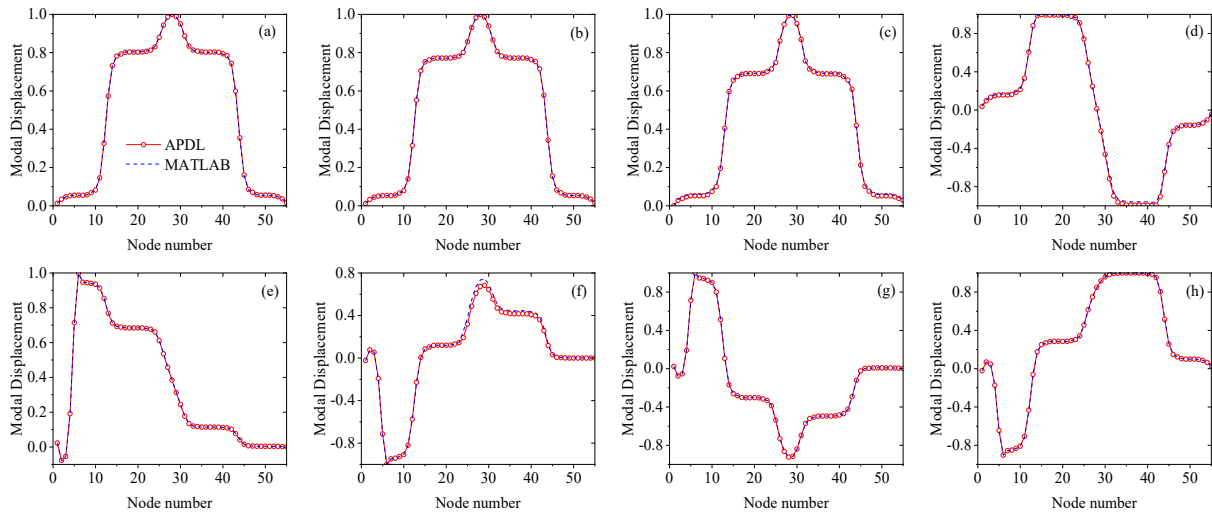
Fig. 8 Modal displacement calculated by APDL and MATLAB: (a) first-order mode (healthy), (b) second-order mode (healthy), (c) third-order mode (healthy), (d) fourth-order mode (healthy), (e) first-order mode (damaged), (f) second-order mode (damaged), (g) third-order mode (damaged), and (h) fourth-order mode (damaged)
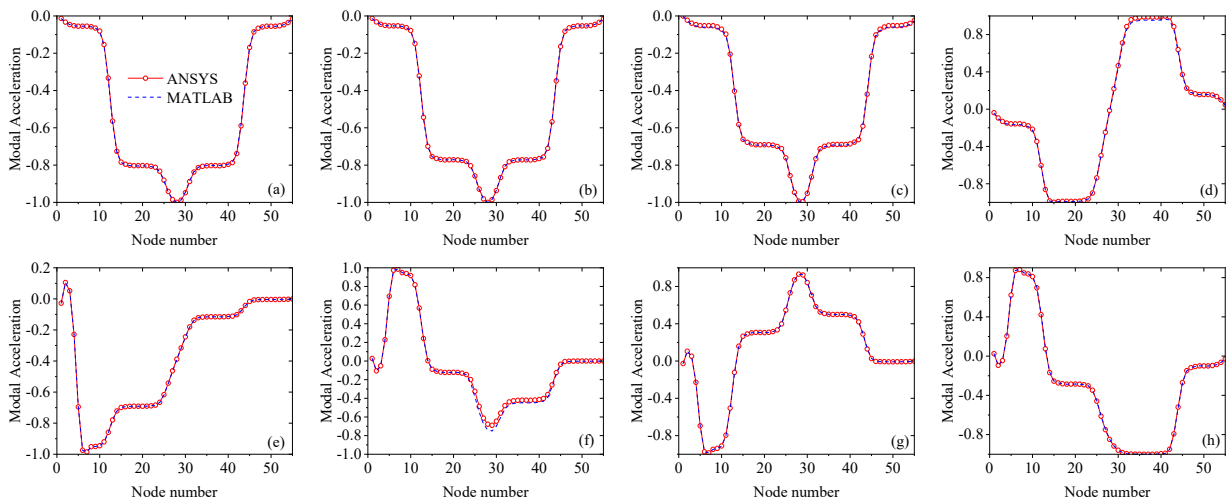
Fig. 9 Modal acceleration calculated by APDL and MATLAB: (a) first-order mode (healthy), (b) second-order mode (healthy), (c) third-order mode (healthy), (d) fourth-order mode (healthy), (e) first-order mode (damaged), (f) second-order mode (damaged), (g) third-order mode (damaged), and (h) fourth-order mode (damaged)

    The results in Tables 2 and 3 and Figs. 8 and 9 show that the natural frequencies obtained are consistent with previous studies and that the two methods (APDL and MATLAB) used to obtain the modal data for the jumper produce consistent results.

4.   Results and discussion

4.1 Single crack identification

    To validate the efficacy of the FDCD method in damage recognition, we analyzed its detection results under the six distinct operating conditions listed in Table 4. Based on the parameter features used by previous researchers and compare analysis, we used a sliding window with five sample points, with a sample distance of 0.1m. Modal displacement and modal acceleration are the two parameters used for identification. Figs. 10 and 11 show the identification results, where KFD$_{MD}$ is modal displacement calculated via the FDCD method and the KFD$_{MA}$ is modal acceleration obtained using the same approach.

Table 4 Single crack damage condition.

Condition number	Damaged node	Degree of damage
OP1	9	10%
OP2	17	10%
OP3	22	10%
OP4	33	10%
OP5	41	10%
OP6	53	10%
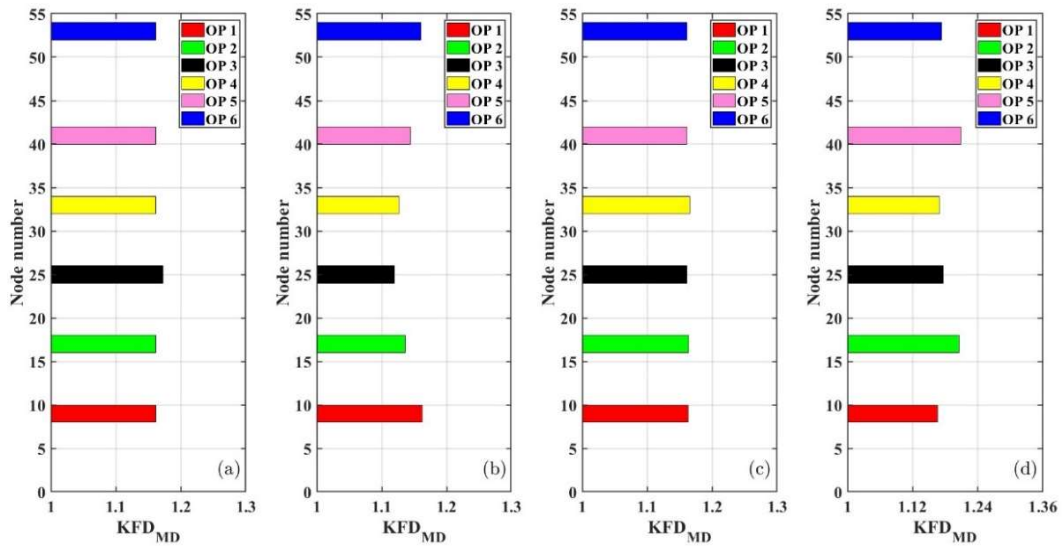
Fig. 10 Damage detection using modal displacement of the first four modes: (a) first-order mode, (b) second-order mode, (c) third-order mode, and (d) fourth-order mode
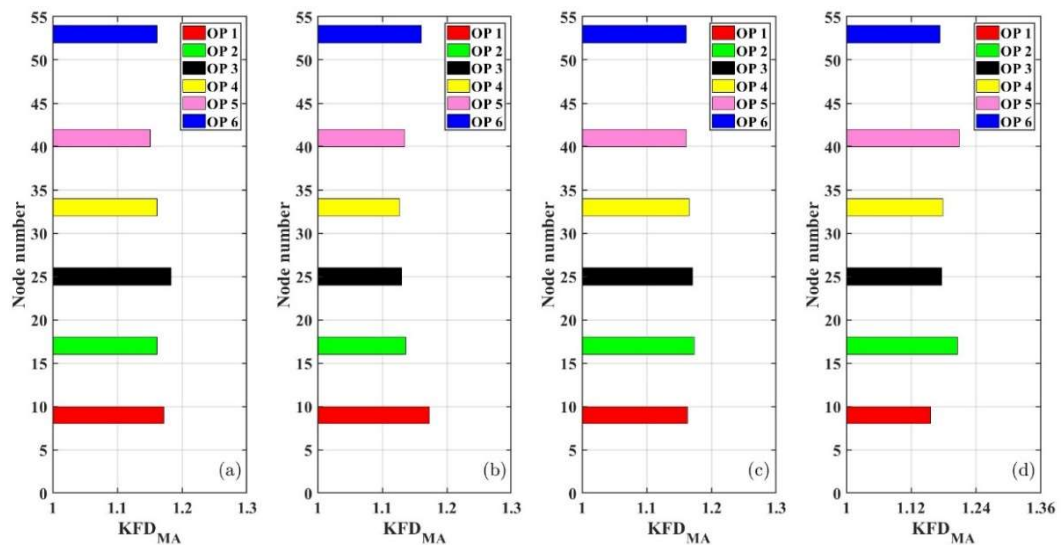
Fig. 11 Damage detection using modal acceleration of the first four modes: (a) first-order mode, (b) second-order mode, (c) third-order mode, and (d) fourth-order mode

Figs. 10 and 11 show that the damaged location can be accurately identified using the above two kinds of data in the first four modes. When using the first-order mode, the effect of damage detection is slightly better in the central region than at either end, which is the opposite of using the second-order mode. The effect of damage detection is optimal when using the fourth-order mode.

4.2 Damage degree detection

To validate the effect of the FDCD method in evaluating the degree of damage, the six positions listed in Table 4 were subjected to identification under varying degrees of damage. Previous studies relied solely on modal displacement for damage degree detection. However, verification of repeated simulations shows that using modal acceleration to detect the degree of damage is not ideal. In addition, the first-order modal displacement is insensitive to the degree of damage. Consequently, this study uses the second-order modal displacement to detect the degree of damage.
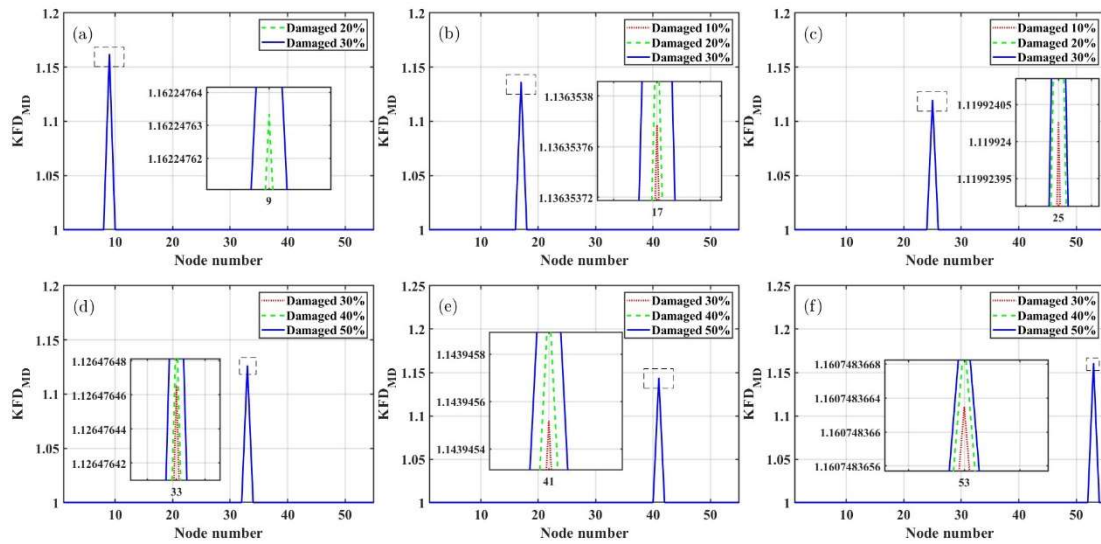
Fig. 12 Modal displacement is used to identify the degree of damage: (a) damaged node 9, (b) damaged node 17, (c) damaged node 22, (d) damaged node 33, (e) damaged node 41, and (f) damaged node 53

Fig. 12 shows the effectiveness of the FDCD method in assessing the degree of damage. The results show that, with increasing damage, the peak value increases under each condition. Notably, the recognition stability at the two ends exceeds that at the central region.

4.3 Identification of multiple cracks

This section verifies the effectiveness of the FDCD method in the presence of multiple cracks across the jumper. The identification was under the four working conditions listed in Table 5.

Table 5 Multiple cracks damage conditions.

Condition number	Damaged node & degree
OP1	9(10%), 17(30%)
OP2	17(10%), 33(30%)
OP3	33(30%), 41(10%)
OP4	25(30%), 53(10%)

For the jumper, the first two modes reveal the structural features and flexibility of the system. During the identification process, the recognition effect of the damaged location of double cracks is significant. However, if a crack occurs near a flexible portion of the structure, the peak value of damage tends to be increased, resulting in inaccurate identification of the damage degree between multiple cracks.

To address this issue, we applied the modal anomaly recognition algorithm proposed by [20] to the Katz fractal dimension (KFD-MAA). The principle of this algorithm is to map modal parameters to another vector space, preserving complete structural attributes while eliminating the influence of structural flexibility. The formula for the KFD-MAA is:

$$\begin{bmatrix} x_i^* \\ y_i^* \end{bmatrix} = \begin{bmatrix} 1 & 0 \\ \sin a & \cos a \end{bmatrix} \begin{bmatrix} x_i \\ y_i \end{bmatrix} \qquad (i=1,2,3,\cdots,n) \qquad (32)$$

where $-\dfrac{\pi}{2} < a < \dfrac{\pi}{2}$, $\begin{bmatrix} 1 & 0 \\ \sin a & \cos a \end{bmatrix}$ is a bijective linear mapping, and (x_i, y_i) and (x_i^*, y_i^*) are the original modal parameters and the mapped modal parameters, respectively.

Figs. 13 and 14 show the results for multiple cracks identified by using the KFD-MAA method.
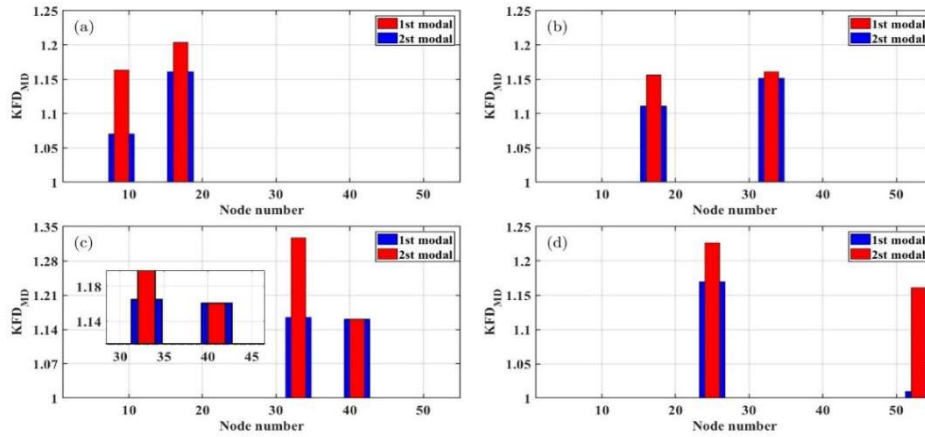
Fig. 13 Modal displacement used for damage detection: (a) first- and second-order modes (OP1), (b) first- and second-order modes (OP2), (c) first- and second-order modes (OP3), and (d) first- and second-order modes (OP4)
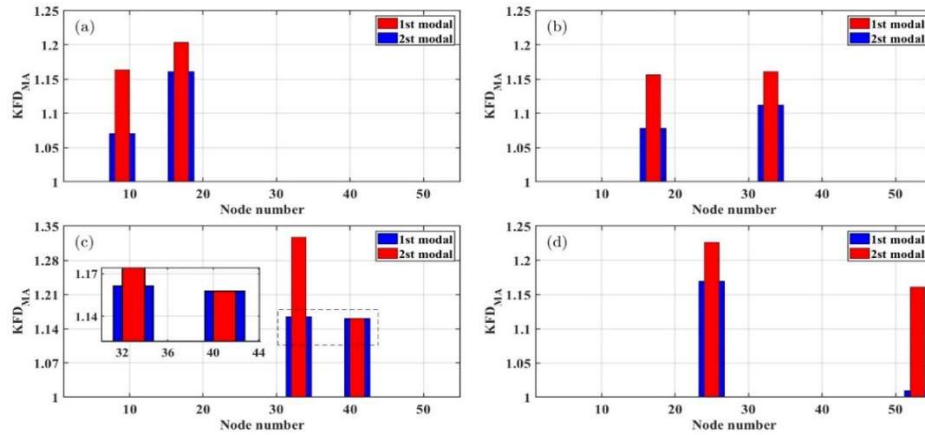
Fig. 14 Modal acceleration used for damage detection: (a) first- and second-order modes (OP1), (b) first- and second-order modes (OP2), (c) first- and second-order modes (OP3), and (d) first- and second-order modes (OP4)

Figs. 13 and 14 show that using the first-order data for identification may result in a significantly higher peak for one of the damaged nodes, leading to indistinct peaks for other nodes. However, using the second-order data for identification avoids this problem.

4.4 Crack identification under noisy conditions

When operating in the seabed environment, obtained signals about the jumper are inevitably affected by noise due to the complexity of the environment. This section investigates the robustness of using the FDCD method for damage detection. Zhu et al. [38] reported that the signal-to-noise ratio (*SNR*) for monitoring subsea pipelines typically ranges from 60 to 100 dB. We add Gaussian white noise with a *SNR* of 30 dB to the modal data to further evaluate the robustness. The six working conditions listed in Table 4 are used for identification.

SNR is given by the logarithm of the ratio of signal power to noise power:

$$SNR = 10 \times \log_{10}(\frac{P_{signal}}{P_{noise}}) \tag{33}$$

Due to the discrete nature of the signals collected, the signal power can be calculated directly by summing. Assuming that the signal is $S = \{s_1, s_2, \cdots, s_n\}$, then the signal power is:

$$P_{signal} = \frac{1}{n}\sum_{i=1}^{n} s_i^2 \tag{34}$$

After calculating the signal power, the noise power to add is calculated based on the *SNR* as:

$$P_{noise} = \frac{P_{signal}}{10^{\frac{SNR}{10}}} \tag{35}$$
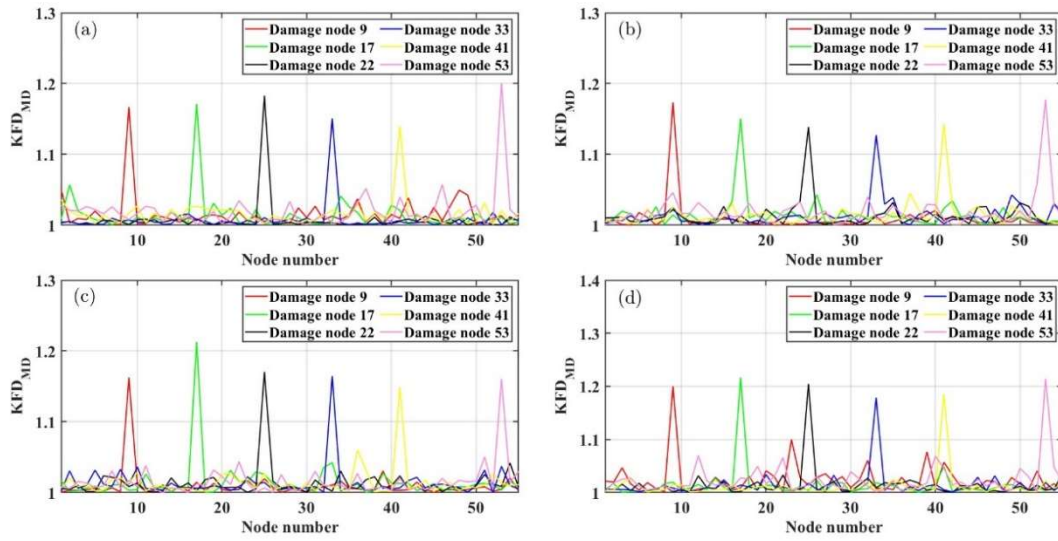
Fig. 15 Damage detection based on the first four displacement modes with noise: (a) first-order mode, (b) second-order mode, (c) third-order mode, and (d) fourth-order mode
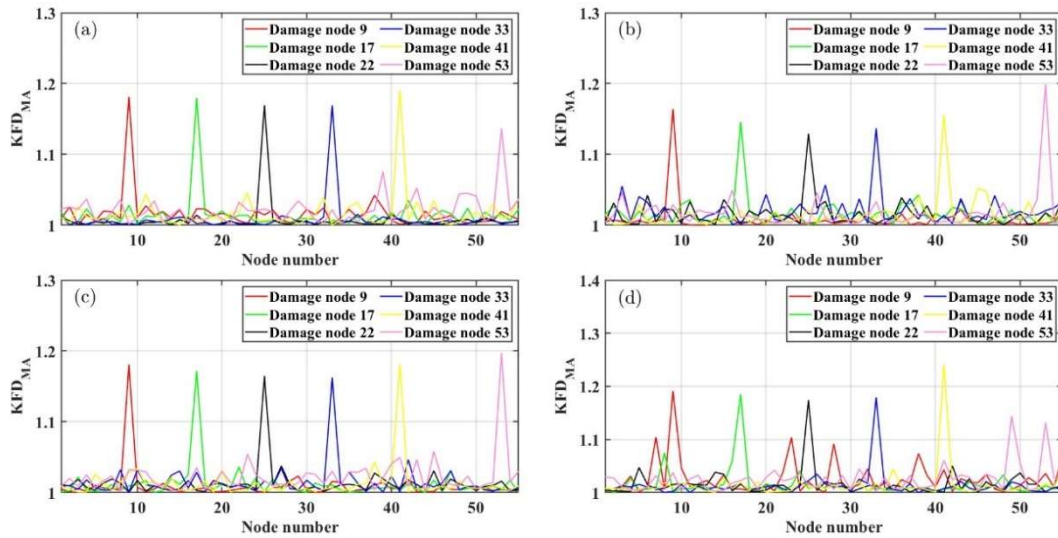
Fig. 16. Damage detection based on the first four acceleration modes with noise: (a) first-order mode, (b) second-order mode, (c) third-order mode, and (d) fourth-order mode.

Figs. 15 and 16 show the results of using the FDCD method to detect damage in the presence of noise. Figs. 15 and 16 indicate that the damaged area is accurately located even in the presence of significant noise.

14

When using the first four modal orders for recognition, the damage in the central region is identified more accurately than at the two ends. These results indicate the robustness of the central region in damage detection is stronger.

5. Conclusion

This study uses fractal theory to detect the structural damage of the subsea jumper based on modal characteristics. A comprehensive investigation is conducted on the recognition performance under various damage conditions. Some new and original conclusions were drawn as follows:

(1) With respect to previous methods, the proposed method improves the accuracy with which the location and degree of jumper damage are detected and is relatively insensitive to noise. The results indicate that cracks even with a depth of 0.2mm can be effectively identified.

(2) Comparing the detection of different damage conditions indicates that the fourth-order modal parameter is more effective than the first three modal parameters for identifying a single crack. The identification effect of the central region of the first-order parameter is slightly better than either end, while the opposite is true for the second-order parameter. Moreover, the detection effect of the damage degree at both ends is more accurately identified than that in the central region.

(3) For multiple cracks, the identification efficacy of the second-order modal parameters surpasses the first-order parameters. In the presence of noise, the central region exhibits stronger robustness.

Acknowledgements

Appendix A. Schematic diagram of subsea jumpers cracking model
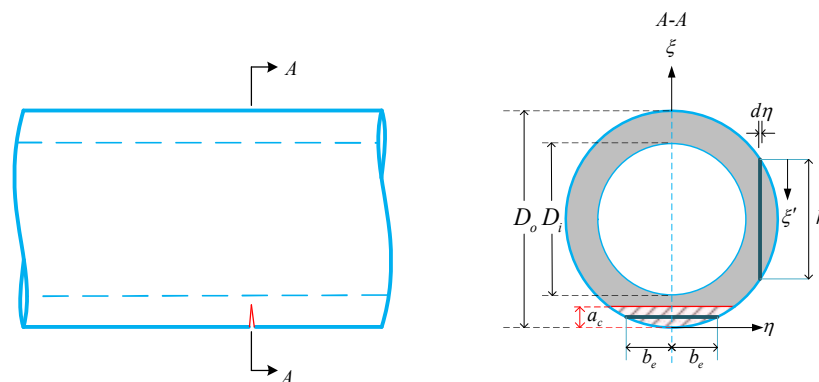
Fig. A.1. Diagram of crack in jumper surface.
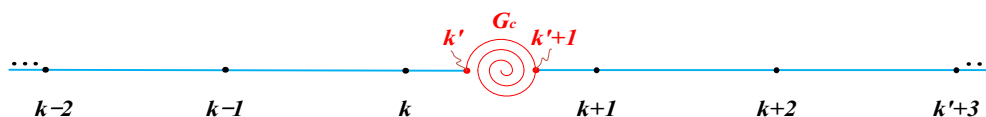
Fig. A.2. Equivalent cracked model of a torsional spring.

REFERENCES

[1]   Bruschi, R., Parrella, A., Vignati, G. C., Vitali, L., 2017. Crucial issues for deep water rigid jumper design. *Ocean Engineering*, 137, 193–203. https://doi.org/10.1016/j.oceaneng.2017.03.059

[2]   Zareei, M. R., Iranmanesh, M., 2018. Reliability-based inspection planning of the ship structure exposed to fatigue damages.

Brodogradnja, 69(2), 119-134. https://doi.org/10.21278/brod69208

[3]   Sorić, J., Lesičar, T., Putar, F., Tonković, Z., 2021. On multiscale damage modelling of heterogeneous materials using nonlocal continuum theory. *Brodogradnja*, 72(4), 121-139. https://doi.org/10.21278/brod72407

[4]   Li, W., Zhou, Q., Yin, G., Ong, M. C., Li, G., Han, F., 2022. Experimental investigation and numerical modeling of two-phase flow development and flow-induced vibration of a multi-plane subsea jumper. *Journal of Marine Science and Engineering*, 1334, 1-24. https://doi.org/10.3390/jmse10101334

[5]   Alkan, S., 2022. Enhancement of marine corrosion and tribocorrosion resistance of offshore mooring chain steel by aluminizing process. *Brodogradnja*, 73(4), 131-159. https://doi.org/10.21278/brod73407

[6]   Zhou, X., Chen, J., Ge Z., Zhao, T., Li, W., 2022. Numerical investigations on the effects of seabed shallow soils on a typical deepwater subsea wellhead system. *Brodogradnja*, 73(3),1-19. http://dx.doi.org/10.21278/brod73301

[7]   Cawley, P., Adams, R. D., 1979. The location of defects in structures from measurements of natural frequencies. *The Journal of Strain Analysis for Engineering Design*, 14(2), 49-57. https://doi.org/10.1243/03093247V142049

[8]   Pandey, A. K., Biswas, M., Samman, M. M., 1991. Damage detection from changes in curvature mode shapes. *Journal of Sound and Vibration*, 145(2), 321–332. https://doi.org/10.1016/0022-460X(91)90595-B

[9]   Shi, Z. Y., Law, S. S., Zhang, L. M., 1998. Structural damage localization from modal strain energy change. *Journal of Sound and Vibration*, 218(5), 825–844. https://doi.org/10.1006/jsvi.1998.1878

[10] Seyedpoor, S. M., 2012. A two stage method for structural damage detection using a modal strain energy based index and particle swarm optimization. *International Journal of Non-Linear Mechanics*, 47(1), 1–8. https://doi.org/10.1016/j.ijnonlinmec.2011.07.011

[11] Alavinezhad, M., Hassanabad, M. G., Ketabdari, M. J., Masoud, N., 2022. Numerical and experimental structural damage detection in an offshore flare bridge using a proposed modal strain energy method. *Ocean Engineering*, 252, 111055. https://doi.org/10.1016/j.oceaneng.2022.111055

[12] Liu G., Zhai Y., Leng D., Tian X., Mu W., 2017. Research on structural damage detection of offshore platforms based on grouping modal strain energy. *Ocean Engineering*, 140: 40-49. https://doi.org/10.1016/j.oceaneng.2017.05.021

[13] Wang, N., Zhu, R., Wang, Q., Zheng, J., Zhang, J., 2022. A method for quantitative damage identification in a high-piled wharf based on modal strain energy residual variability. *Ocean Engineering*, 254, 111314. https://doi.org/10.1016/j.oceaneng.2022.111314

[14] Muc, A., Murawski, L., Szeleziński, A., 2018. Methods of cracks detection in marine structures' welded joints based on signals' time waveform analysis. *Brodogradnja*, 69(3), 43-59. https://doi.org/10.21278/brod69303

[15] Mironovs, D., Ručevskis, S., Dzelzītis, K., 2022. Prospects of structural damage identification using modal analysis and anomaly detection. *Procedia Structural Integrity*, 37, 410-416. https://doi.org/10.1016/j.prostr.2022.01.103

[16] Zhou, L., Wang, P., Zhang, C., Qu, X., Gao, C., Xie, Y., 2022. Multi-mode fusion BP neural network model with vibration and acoustic emission signals for process pipeline crack location. *Ocean Engineering*, 264, 112384. https://doi.org/10.1016/j.oceaneng.2022.112384

[17] Je, H. M., Park, S. Y., 2015. A study on damage detection of production riser. *Journal of Naviation and Port Research*, 39(3), 179–184. https://doi.org/10.5394/KINPR.2015.39.3.179

[18] Min, C., Kim, H., Yeu, T., Hong, S., 2015. Sensitivity-based damage detection in deep water risers using modal parameters: numerical study. *Smart Structure and Systems*, 15(2), 315–334. https://doi.org/10.12989/sss.2015.15.2.315

[19] Sivaprasad, H., Lekkala, M. K. R., Latheef, M., Seo, J., Yoo, K., Jin, C., Kim, D. K., 2023. Fatigue damage prediction of top tensioned riser subjected to vortex-induced vibrations using artificial neural networks. *Ocean Engineering*, 268, 113393. https://doi.org/10.1016/j.oceaneng.2022.113393

[20] Zhou, X., Wang, D., Duan, M., Gu, J., Liu, Y., 2017. Numerical study on mode curvature for damage detection of a drilling riser using transfer matrix technique. *Applied Ocean Research*, 63, 65–75. https://doi.org/10.1016/j.apor.2016.12.008

[21] Zhou, X., Sun, Y., Duan, M., Li, W., 2020. Numerical investigation on crack identification using natural frequencies and mode shapes of a drilling riser during deployment and retrieval. *Journal of Petroleum Science and Engineering*, 195, 107721. https://doi.org/10.1016/j.petrol.2020.107721

[22] Bayik, B., Omenzetter, O., Pavlovskaia, E., 2020. Experimental modelling of a top-tensioned riser for vibration-based damage detection. *Engineering Structures*, 223, 111139. https://doi.org/10.1016/j.engstruct.2020.111139

[23] Hadjileontiadis, L. J., Douka, E., Trochidis, A., 2005. Fractal dimension analysis for crack identification in beam structures. *Mechanical Systems and Signal Processing*, 19, 659-674. https://doi.org/10.1016/j.ymssp.2004.03.005

[24] Qiao, P., Cao, M., 2008. Waveform fractal dimension for mode shape-based damage identification of beam-type structures. *Solids and Structures*, 45, 5946-5961. https://doi.org/10.1016/j.ijsolstr.2008.07.006

[25] Bai, R., Cao, M., Su, Z., Ostachowicz, W., Xu, H., 2012. Fractal dimension analysis of higher-order mode shapes for damage identification of beam structures. *Mathematical Problems in Engineering*, 454568. https://doi.org/10.1155/2012/454568

[26] Huang, Y., Li, H., Wu, S., Yang, Y., 2018. Fractal dimension based damage identification incorporating multi-task sparse

Bayesian learning. *Smart Materials and Structures*, 27(7), 075020. https://doi.org/10.1088/1361-665X/aac248

[27]   Kleivane, S., Leira, B., Steen S., 2023. Development of a reliability model for crack growth occurrence for a secondary hull component. *Brodogradnja*, 74(1), 99-115. http://dx.doi.org/10.21278/brod74106

[28]   Li, W., Song, W., Yin, G., Ong, M. C., Han, F., 2022. Flow regime identification in the subsea jumper based on electrical capacitance tomography and convolution neural network. *Ocean Engineering*, 266, 113152. https://doi.org/10.1016/j.oceaneng.2022.113152

[29]   API Spec 5L, 2018. Specification for Line Pipe. Forty-fifth Edition.

[30]   Qu, Y., Fu, S., Liu, Z., Xu, Y., Sun, J., 2022. Numerical study on the characteristics of vortex-induced vibrations of a small-scale subsea jumper using a wake oscillator model. *Ocean Engineering*, 243, 110028. https://doi.org/10.1016/j.oceaneng.2021.110028

[31]   Zheng, D. Y., Fan, S. C., 2003. Vibration and stability of cracked hollow-sectional beams. *Journal of Sound and Vibration*, 267(4), 933–954. https://doi.org/10.1016/S0022-460X(02)01605-X

[32]   Labib, A., Kennedy, D., Featherston, C., 2014. Free vibration analysis of beams and frames with multiple cracks for damage detection. *Journal of Sound and Vibration*, 333(20), 4991–5003. https://doi.org/10.1016/j.jsv.2014.05.015

[33]   Yashar, A., Ferguson, N., Ghandchi-Tehrani, M., 2018. Simplified modelling and analysis of a rotating Euler-Bernoulli beam with a single cracked edge. *Journal of Sound and Vibration*, 420, 346–356. https://doi.org/10.1016/j.jsv.2017.12.041

[34]   Mandelbrot, B. B., 1982. The Fractal Geometry of Nature. New York, NY, USA,6-19.

[35]   Zhou, X., Li, Y., Chen, J., Li, W., Duan, M., 2022. Numerical evaluation of the coupled/uncoupled effects of lower marine riser package and/or blowout preventer with a lower flex joint in a hang-off drilling riser. *Ocean Engineering*, 266, 113004. https://doi.org/10.1016/j.oceaneng.2022.113004

[36]   Wang, H., Huang, J., Lee, S., Gioielli, P., Kan, W., Spencer, D., Islam, M., 2013. VIV response of a subsea jumper in uniform current. *Proceedings of the ASME 2013 32nd International Conference on Ocean, Offshore and Arctic Engineering*, 9-14 June, Nantes, France, 1-10. https://doi.org/10.1115/OMAE2013-11417

[37]   Zheng, H., Slocum, S. T., Huang, J. Z., Srivastava, V., Lee, S., Wang, H. H., 2015. Numerical analysis of experimental data of subsea jumper vortex induced vibrations. *Proceedings of the ASME 2015 34th International Conference on Ocean, Offshore and Arctic Engineering*, 31 May – 5 June, St. John's, Newfoundland, Canada, 1-14. https://doi.org/10.1115/OMAE2015-41224

[38]   Zhu, H., Du, Z., Tang, Y., 2022. Numerical study on the displacement reconstruction of subsea pipelines using the improved inverse finite element method. *Ocean Engineering*, 248, 110763. https://doi.org/10.1016/j.oceaneng.2022.110763